IEEE Photonics Journal
An IEEE Photonics Society Publication

Open Access

Vector Nature of Dissipative-Soliton-Resonance Pulses in Fiber Lasers Mode-Locked by Nonlinear Polarization Rotation Technique

Volume 11, Number 3, June 2019

Wenxiong Du
Heping Li
Junwen Li
Zhuang Wang
Pinghe Wang
Zhiyao Zhang
Yong Liu

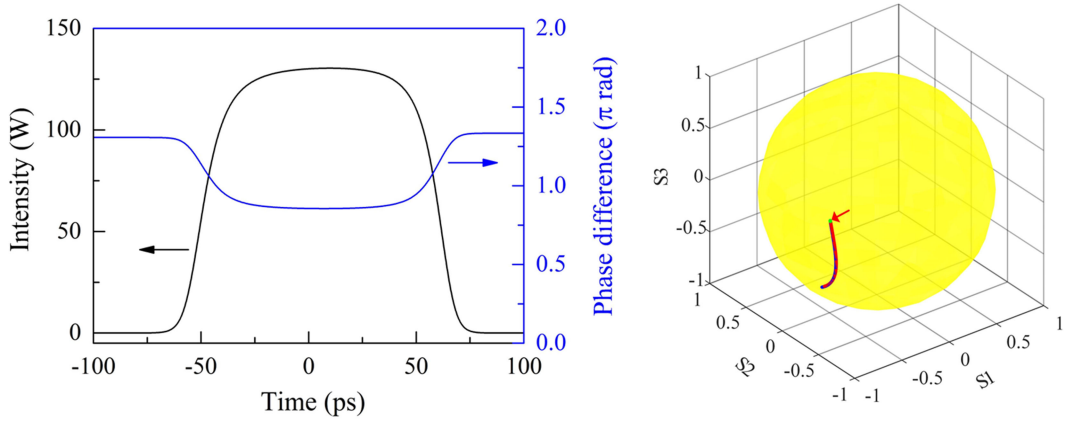

DOI: 10.1109/JPHOT.2019.2918804
1943-0655 © 2019 IEEE

Vector Nature of Dissipative-Soliton-Resonance Pulses in Fiber Lasers Mode-Locked by Nonlinear Polarization Rotation Technique

Wenxiong Du, Heping Li, Junwen Li, Zhuang Wang, Pinghe Wang, Zhiyao Zhang, and Yong Liu

State Key Laboratory of Electronic Thin Films and Integrated Devices, School of Optoelectronic Science and Engineering, University of Electronic Science and Technology of China, Chengdu 610054, China

DOI:10.1109/JPHOT.2019.2918804

Manuscript received January 30, 2019; revised May 13, 2019; accepted May 21, 2019. Date of publication May 24, 2019; date of current version June 4, 2019. This work was supported in part by the National Natural Science Foundation of China under Grant 61775031, Grant 61435003, Grant 61421002, and Grant 61875033 and in part by the National Key R&D Program of China (2016YFF0102003). Corresponding author: Heping Li (e-mail: oehpli@uestc.edu.cn).

Abstract: The vector nature of dissipative-soliton-resonance (DSR) pulses is numerically investigated in an all-normal-dispersion Yb-doped fiber laser mode-locked by the nonlinear polarization rotation technique. We calculate the polarization ellipses of the DSR pulse throughout the cavity, which shows that the polarization state varies during the propagation. The features of pulse polarization are also displayed on the Poincaré sphere. The impact of nonlinear birefringence on the polarization evolution is analyzed. Furthermore, we find that the polarization state is not uniform across a DSR pulse at a fixed intracavity position. The flat-top part of the pulse has a nearly fixed polarization, while its leading and trailing edges feature polarization states that vary with time. The peak power ratio of the two orthogonal polarization components in the pulse is limited in the range from 4 to 31. Our simulation results offer insight into the polarization properties of DSR pulses in mode-locked fiber lasers containing polarization discrimination devices.

Index Terms: Dissipative-soliton-resonance, mode-locked fiber lasers, polarization dynamics.

1. Introduction

Ultrafast fiber lasers have attracted great attention due to their diverse practical applications in optical communications, micromachining, and frequency metrology [1]. To date, numerous passive mode-locking techniques, such as nonlinear polarization rotation (NPR), nonlinear optical loop mirror (NOLM), and real saturable absorbers (SAs), have been exploited for ultrashort-pulse generation. In addition to their widespread use as ultrashort-pulse sources, ultrafast fiber lasers are also regarded as convenient test-beds for the fundamental exploration of complex soliton dynamics. The term soliton refers to special kinds of wave packets that remain intact even after mutual collisions. Since then, solitons have been discovered and investigated in many branches of physics. In the context of optics, Mollenauer *et al*. first demonstrated optical solitons in single-mode fibers (SMFs) [2]. A basic equation that governs the propagation of solitons in SMFs is the nonlinear Schrödinger

equation (NLSE). However, it was found that optical solitons can also exist in non-conservative systems, such as ultrafast fiber lasers. Different from the classical solitons observed in SMFs, the dynamics of solitons formed in fiber lasers can be well described by the complex Ginzburg-Landau equation (CGLE), which takes account not only of the dispersion and nonlinearity but also of the gain and loss. In the past decades, various soliton dynamics have been reported in ultrafast fiber lasers by adjusting the cavity parameters. When a mode-locked fiber laser is constructed with purely anomalous group-velocity dispersion (GVD) fibers, conventional solitons (CSs) can be obtained as a balance between negative GVD and self-phase modulation effects [3]. The technique of dispersion management is often utilized in the design of stretched-pulse fiber lasers [4], where segments of fibers with opposite signs of GVD parameters are combined to reduce the net cavity dispersion to near zero. The pulse stretches and compresses alternately during the propagation, which can decrease the accumulated nonlinear phase shift in the cavity. By changing the cavity dispersion to large-positive or even all-normal dispersion, dissipative solitons (DSs) have been observed [5]. In contrast to the CSs, the formation of DSs is a composite balance involving dissipative and dispersive effects. Pulse shaping in normal-dispersion fiber lasers is attributed to spectral filtering of highly-chirped pulse and the output spectrum exhibits steep edges.

Chang *et al*. have found a new type of DS known as dissipative soliton resonance (DSR) by solving the CGLE [6]. The DSR pulse features a flat-top temporal profile. It shows that with the increase of pump power, the pulse duration can be increased indefinitely without pulse break-up while its peak power remains constant. A number of theoretical studies have subsequently been reported within the framework of the CGLE model [7]–[10]. Based on the lumped model, the mechanism of DSR-pulse generation in mode-locked fiber lasers has been investigated numerically [11]–[13]. DSR phenomena have also been experimentally demonstrated in fiber lasers mode-locked by NPR [14], [15], NOLM [16], [17], and real SAs [18]–[20]. However, emphasis has been given to scalar DSR, neglecting the vector nature of DSR pulses. In practice, a SMF is always weakly birefringent due to manufacturing imperfections, bending or externally applied stress, etc. It can support two degenerate modes that are polarized along both principal axes of the birefringent fiber. Owing to nonlinear coupling, two orthogonal polarization components of a soliton can propagate as a unit. The entity of the coupled soliton is referred to as vector soliton (VS). So far, various types of VSs, including the group velocity-locked (GVL) VSs [21], [22], the polarization rotation-locked (PRL) VSs [23], [24], and the polarization-locked (PL) VSs [25], [26], have been confirmed in mode-locked fiber lasers. Recently, the generation of GVL-DSR pulses has been reported in a figure-of-eight fiber laser [27]. Li *et al*. investigated the internal polarization dynamics of DSR pulses in an Yb-doped fiber laser mode-locked by NOLM [28]. However, since the polarizer and analyzer are required for the implementation of NPR technique, it is worth investigating the vector characteristics of DSR pulses in NPR mode-locked fiber lasers. The exploration of this issue would enrich the VS dynamics in mode-locked fiber lasers with polarization discrimination devices.

In this paper, we report numerical simulations on the vector nature of DSR pulses in an all-normal-dispersion (ANDi) Yb-doped fiber laser mode-locked by the NPR technique. The polarization ellipses of the DSR pulse inside the laser cavity were calculated. The features of pulse polarization were also shown on the Poincaré sphere. The influence of nonlinear birefringence on the polarization evolution is discussed. We also analyzed the internal polarization dynamics of DSR pulses. The peak power ratio of the two orthogonal polarization modes in the DSR pulse was given as a function of the orientation angles of polarization-dependent components in the cavity.

2. Numerical Model

The proposed ANDi Yb-doped mode-locked fiber laser is schematically shown in Fig. 1. The laser cavity is composed of a 4 m Yb-doped fiber (YDF), a polarization-dependent isolator (PD-ISO), a Gaussian-shaped spectral filter with a bandwidth of 14 nm, a polarization controller (PC), two pieces of SMFs with a total length of 24 m, and a 50:50 output coupler (OC). The cavity length L is 28 m. The dispersion parameters of the fibers are $\beta_{2,YDF} = 20$ ps^2/km and $\beta_{2,SMF} = 23$ ps^2/km, respectively. The net cavity dispersion is 0.632 ps^2. All the fibers are assumed to have the same

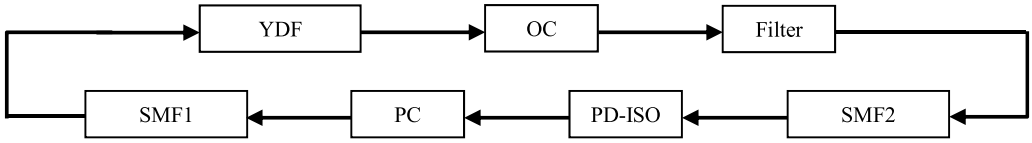

Fig. 1. Schematic of an all-normal-dispersion Yb-doped mode-locked fiber laser.

nonlinear coefficient of $\gamma = 3\ \mathrm{W^{-1}km^{-1}}$. The PD-ISO has the functions of both the polarizer and analyzer while the PC introduces a linear phase delay bias Φ_{ph} between the two polarization modes in the pulse. The PD-ISO together with the PC acts as a mode locker, which is needed to initiate mode locking and to stabilize the pulse through suppressing the generation of cavity background noise.

In contrast to the CGLE model where a small-pulse-variation approximation was assumed, we numerically simulated the pulse formation and evolution in the laser based on a cavity round-trip model [29]. The action of each cavity element on the pulse was considered. Pulse propagation in a linearly birefringent fiber can be described by the following coupled Ginzburg-Landau equation

$$\begin{aligned}\frac{\partial u}{\partial Z} &= i\beta u - \delta\frac{\partial u}{\partial T} - i\frac{\beta_2}{2}\frac{\partial^2 u}{\partial T^2} + i\gamma\left(|u|^2 + \frac{2}{3}|v|^2\right)u + i\frac{\gamma}{3}v^2u^* + \frac{g}{2}u + \frac{g}{2\Omega_g^2}\frac{\partial^2 u}{\partial T^2},\\ \frac{\partial v}{\partial Z} &= -i\beta v + \delta\frac{\partial v}{\partial T} - i\frac{\beta_2}{2}\frac{\partial^2 v}{\partial T^2} + i\gamma\left(|v|^2 + \frac{2}{3}|u|^2\right)v + i\frac{\gamma}{3}u^2v^* + \frac{g}{2}v + \frac{g}{2\Omega_g^2}\frac{\partial^2 v}{\partial T^2},\end{aligned} \tag{1}$$

where u and v denote the normalized envelopes of the pulse polarized along the slow and fast axis of the birefringent fiber, respectively; $2\beta = 2\pi/L_b$ is the wave-number difference between the two polarization components, and L_b is the beat length; $2\delta = 2\beta\lambda/2\pi c$ is the inverse group-velocity difference; β_2 represents the GVD parameter of fiber; γ refers to the nonlinearity coefficient of fiber; g describes the gain function of the YDF; Ω_g denotes the gain bandwidth, which is set to 30 nm. For the SMFs, $g = 0$ and the last two terms on the right side of Eq. (1) are ignored. For the YDF, the gain saturation effect is considered as

$$g = g_0\ \exp\left[-\frac{\int(|u|^2 + |v|^2)dt}{E_{sat}}\right], \tag{2}$$

where g_0 is the small signal gain, which is related to the doping concentration; E_{sat} is the gain saturation energy and the increase of E_{sat} is equivalent to increasing the pump power. In our simulations, g_0 is fixed at 2 $\mathrm{m^{-1}}$ and E_{sat} is variable.

The effects of other discrete cavity elements, such as the PC, the OC, and the PD-ISO, were simulated by multiplying their corresponding transfer matrixes with the optical field whenever the pulse encounters them. For the simplicity, we assumed that different pieces of fibers inserted in the cavity have the same principal axes. Actually, by setting the polarizer and analyzer to have different orientation angles θ and φ with respect to the fast axis of the birefringent fiber, the impact caused by the possible non-coincidence of the fiber axes has been taken into account. Due to the complexity of the model, we utilized the split-step Fourier method to solve it numerically. In the simulations, we started the calculation from an arbitrary weak pulse. After a round-trip propagation in the cavity, we then used the final optical field as an input for the next round of calculation. Eventually, a steady state could always be obtained under appropriate operation conditions.

An approach to describing the polarization evolution of a pulse formed in the cavity is based on motion of the Stokes vector on the Poincaré sphere. At this point, four variables known as the Stokes parameters are introduced and defined as

$$\begin{aligned}&S_0 = |u|^2 + |v|^2,\ S_1 = |u|^2 - |v|^2,\\ &S_2 = 2\ |u|\,|v|\cos\Delta\varphi,\ S_3 = 2\ |u|\,|v|\sin\Delta\varphi,\\ &s_i = S_i\Big/\sqrt{{S_1}^2 + {S_2}^2 + {S_3}^2},\ (i-1,2,3)\end{aligned} \tag{3}$$

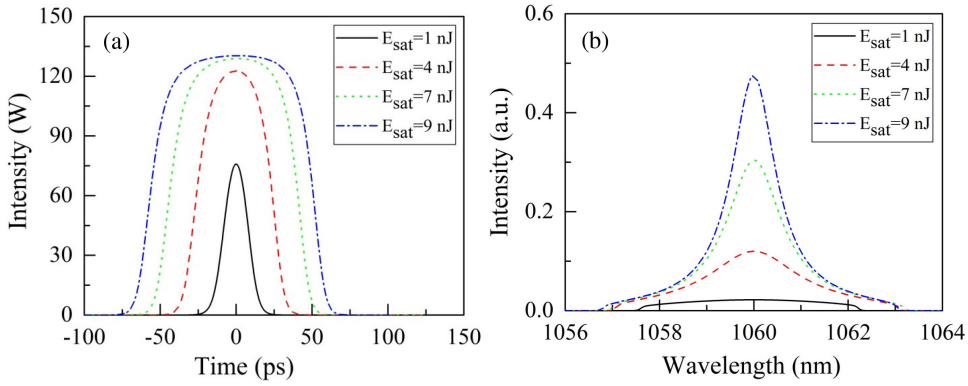

Fig. 2. DSR-pulse generation. (a) Pulse temporal profiles with the increasing E_{sat}. (b) Pulse spectral profiles with the increasing E_{sat}.

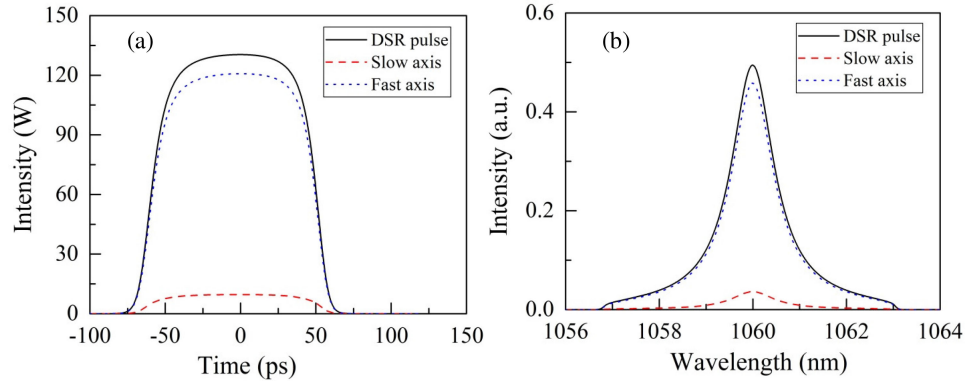

Fig. 3. Simulation results of output pulses. (a) The temporal profiles of the output pulse and its two orthogonal polarization components. (b) The corresponding pulse spectral profiles.

where $\Delta\varphi$ refers to the phase difference between the two polarization modes; s_i is the normalized Stokes parameters. It can be easily verified from Eq. (3) that $s_0^2 = s_1^2 + s_2^2 + s_3^2 = 1$. As s_0 is invariant with time and space, the Stokes vector with components s_1, s_2, and s_3 moves on the surface of a sphere of radius s_0 as the pulse propagates in the cavity, which provides a visual description of the polarization dynamics.

3. Simulation Results and Discussion

In our simulations, when the parameters were set to $L_b = 7$ m (i.e., $L/L_b = 4$), $\theta = 0.1\pi$, $\varphi = 0.3\pi$, and $\Phi_{ph} = 0.75\pi$, stable pulses could be achieved in the cavity. As shown in Fig. 2(a), when the pump E_{sat} is increased from 1 nJ to 9 nJ, the peak power of the output pulse initially increases and then clamps at a certain value while its temporal profile transfers from a Gaussian shape to a rectangular one. Fig. 2(b) illustrates the change in the corresponding pulse spectra. As the pump power is increased, the intensity in the central region of pulse spectrum grows continuously, which results in a bell-shaped top appearing in the rectangular spectral profile. The 3-dB bandwidth is significantly narrowed at first and then keeps almost unchanged. The evolution process from the DS to the rectangular pulse is in agreement with the DSR theory, indicating that stable DSR pulses are generated in the cavity.

Fig. 3 depicts the temporal and spectral profiles of the two polarization modes in the output DSR pulse when E_{sat} is set to 9.2 nJ. As presented in Fig. 3(a), the peak powers of the orthogonally

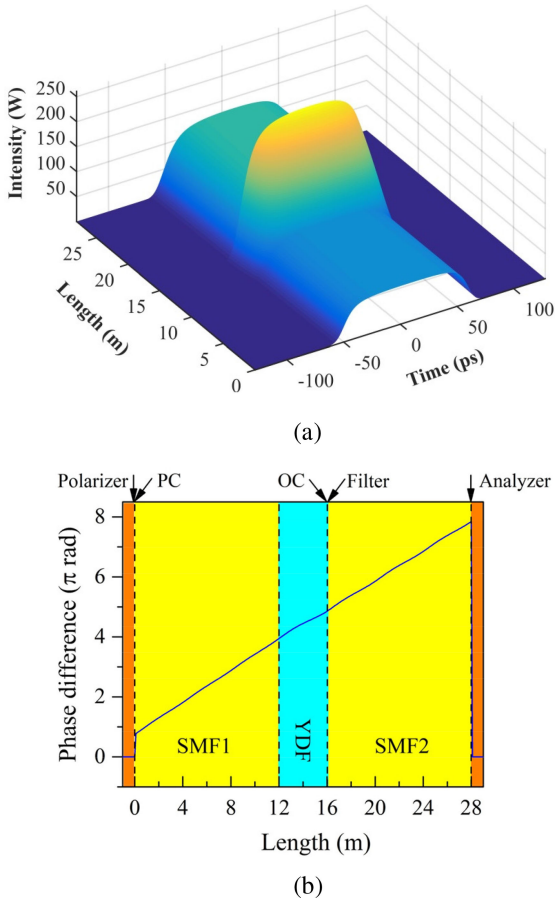

Fig. 4. Intra-cavity DSR-pulse evolution. (a) Three-dimension evolution. (b) Variation of the phase difference between the two components along the cavity.

polarized components are unequal and the strong polarization mode is along the fast axis of the fiber. The peak power ratio of the two components is 12. Fig. 3(b) shows the corresponding pulse spectra, which have the same central wavelength centered at 1060 nm. The characteristics of the intra-cavity DSR-pulse evolution are illustrated in Fig. 4. One can see from Fig. 4(a) that the pulse with a rectangular temporal profile can exist throughout the laser cavity. The relative fluctuation of the pulse duration is quite low during the propagation. Fig. 4(b) illustrates the phase-difference variation between the two components along the cavity. After the pulse passes through the polarizer, the phase difference is locked to 0 rad. As it propagates further in the cavity, the phase difference increases linearly from 0 to 7.85π rad. When the pulse finally traverses the analyzer, the phase difference will change to 0 rad immediately. The actual relative-phase change over one cavity length is thus about 7.85π rad. It is worth noting that if only the linear birefringence is taken into account, the phase difference between the two polarization modes accumulated in a cavity roundtrip should be equal to 8π rad in the case of $L = 4L_b$. The origin of the slight discrepancy between 7.85π and 8π can be understood from the following qualitative explanation. In our simulations, the orientation of the polarizer has an angle of $\theta = 0.1\pi$ from the fast axis of the fiber, and the fast-axis component in the pulse thus has a larger peak power. The nonlinear contribution to the refractive index of the fast axis is greater relative to the slow-axis one, which thereby leads to a reduction of the difference in total indices between the axes. As a result, the fiber becomes less birefringent and the actual beat length increases.

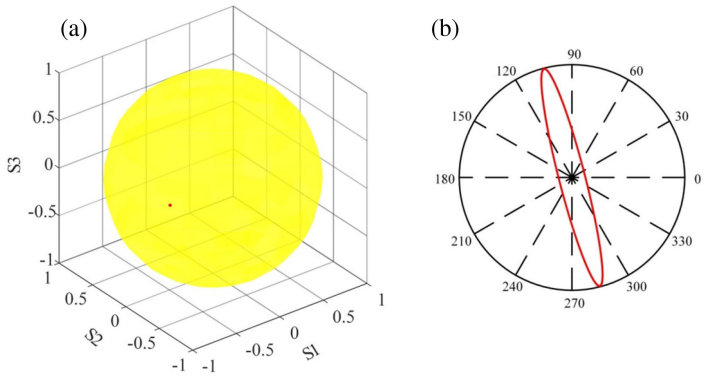

Fig. 5. The polarization evolution of DSR pulses. (a) The polarization evolution of output pulses with cavity roundtrips shown on the Poincaré sphere. (b) The polarization ellipse of the pulse at the position of the OC.

The polarization evolution of output pulses with cavity roundtrips is presented by using the Poincaré sphere, as depicted in Fig. 5(a). A fixed point on the Poincaré sphere implies that the pulse has a stationary polarization state. The polarization ellipse of the pulse at the position of the OC is shown in Fig. 5(b). The pulse is elliptically polarized with its larger axis of polarization near the fast axis of the fiber. We also calculated the polarization ellipses of the pulse at various locations inside the cavity, as illustrated in Fig. 6. Obviously, both the orientation angle and ellipticity of the polarization ellipse vary during the propagation, i.e., the polarization state changes. When the pulse propagates along the fibers, its polarization state is elliptically polarized. The intra-cavity polarizer and analyzer provide a polarization feedback on the pulse circulating in the cavity. After the pulse passes through them, its polarization state will be forced into a linear polarization immediately. As an example, Fig. 6(b) shows the polarization ellipse of the DSR pulse at a position of 7 m in the cavity, and Fig. 6(d) presents the other one after the pulse propagates over L_b. Obviously, the polarization state in Fig. 6(d) does not return to its original one shown in Fig. 6(b). Generally, if only the linear birefringence is taken into consideration, the polarization state of light changes continuously along the fiber in a periodic manner with a period equal to the beat length L_b. However, the polarization evolution of the DSR pulse along the cavity is determined by both the linear and nonlinear birefringence. In our simulations, the peak power of the fast-axis component in the pulse is stronger than that of the slow-axis one, the nonlinear birefringence thus causes a slight increase in the actual cavity beat length. Our numerical results indicate that the polarization ellipse of the pulse is recovered when propagating over about $1.11L_b$.

Actually, the aforementioned polarization evolution is represented by the polarization ellipse of the central point in the pulse envelope. It remains unclear whether or not the polarization states across the pulse are identical. Thus, we further investigated the internal polarization dynamics of DSR pulses at a fixed cavity position. As shown in Fig. 7(a), the phase difference between the two components is not uniform across the pulse. It can be seen from Fig. 7(b) that the leading edge (red curve) and trailing edge (blue curve) of the pulse show a long trajectory on the Poincaré sphere, while its flat-top part converges to a fixed point (green dot). It should be noted that when a CS is formed in a NPR mode-locked fiber laser, its polarization state is invariant with time at a fixed intra-cavity position [30]. However, our simulation results clearly suggest that the DSR pulse does not acquire a single state of polarization. Although the flat-top part of the pulse has a nearly fixed polarization state, its leading and trailing edges feature polarization states that vary with time. Physically speaking, the DSR pulse has a unique instantaneous frequency behavior. Its flat-top part acquires a moderately low linear chirp frequency, whereas the chirp changes exponentially at the edges [31]. Therefore, the phase difference between the two components is nearly fixed across the pulse envelope, except at the edges, where it varies with time. It is the intrinsic frequency chirp

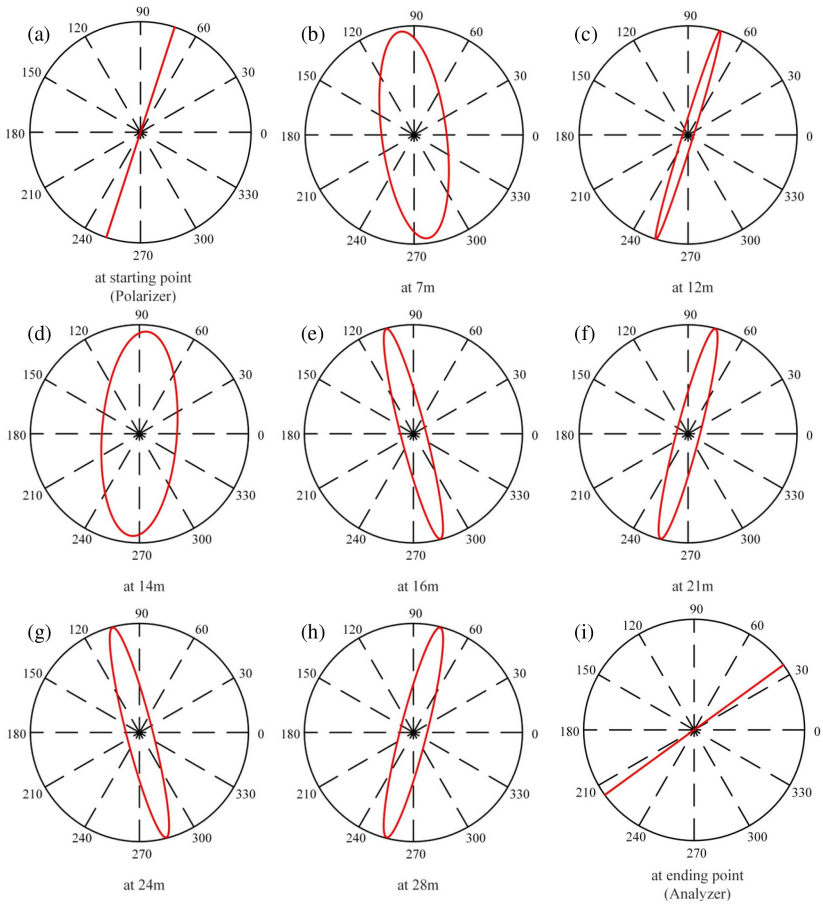

Fig. 6. Polarization ellipses of the DSR pulse at different positions in the cavity.

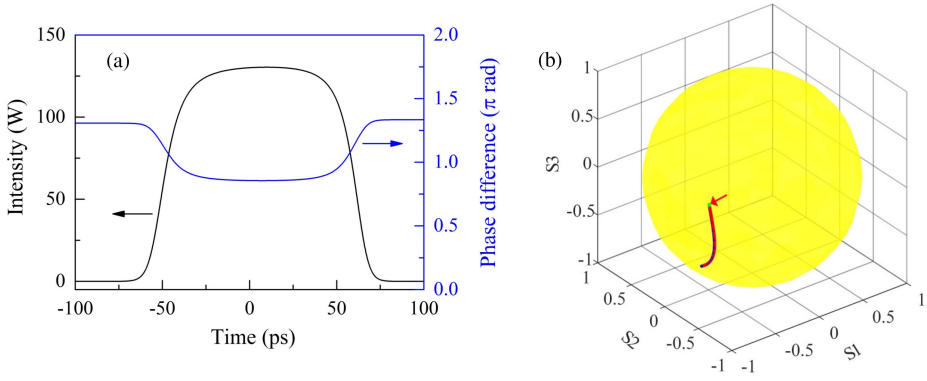

Fig. 7. The internal polarization dynamics of the DSR pulse. (a) The temporal pulse profile (black curve); the phase difference between the two components across the pulse (blue curve). (b) The internal polarization evolution of the pulse shown on the Poincaré sphere; the trajectories of the leading edge (red curve) and trailing edge (blue curve) almost overlap.

property that results in polarization non-uniformity between the flat-top part and edges of the DSR pulse.

Fig. 8 illustrates the existence domain of DSR pulses as a function of orientation angles θ and φ. In this case, we only altered the values of θ and φ while fixing other variables ($L_b = 7$ m, $E_{sat} = 9.2$ nJ,

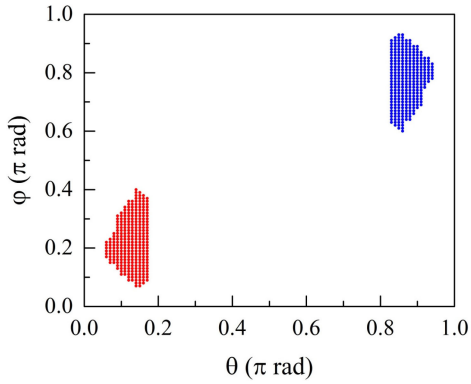

Fig. 8. The existence domain of DSR pulses as a function of orientation angles θ and φ.

and $\Phi_{ph} = 0.75\pi$). It was found that DSR pulses can exist in two regions, as shown in the bottom-left and top-right portions of Fig. 8. In the red region, the orientation angle θ of the polarizer is set in the range from 0.06π to 0.17π, while the analyzer has an angle φ varying from 0.07π to 0.4π. In the blue region, DSR pulses exist in the range where θ and φ vary from 0.83π to 0.94π and 0.6π to 0.93π, respectively.

We noted that if a stable DSR pulse is formed with the orientation angles θ_1 and φ_1, it can also exist in the cavity under the conditions of $\theta = \pi - \theta_1$ and $\varphi = \pi - \varphi_1$. We recall that based on the NPR technique, the intensity-dependent transmission of the cavity can be expressed by

$$T(I) = \sin^2(\theta)\sin^2(\varphi) + \cos^2(\theta)\cos^2(\varphi) + \frac{1}{2}\sin(2\theta)\sin(2\varphi)\cos(\Phi_{ph} + \Phi), \tag{4}$$

where Φ is the phase difference between the two components, which is considered as

$$\Phi = \frac{2\pi L}{L_b} - \frac{\gamma L P}{3}\cos(2\theta), \tag{5}$$

where L is the cavity length and P is the instantaneous peak power of the pulse. It is clear to see from Eqs. (4) and (5) that when other cavity parameters remain unchanged, both the cases of $\theta = \theta_1$ with $\varphi = \varphi_1$ and $\theta = \pi - \theta_1$ with $\varphi = \pi - \varphi_1$ correspond to the same transmission value. This will result in that the DSR pulses obtained in these two cases are identical.

In the existence domain of DSR pulses, we also investigated the peak power ratio R of the two components in the pulse as a function of orientation angles θ and φ, as shown in Figs. 9(a) and 9(b). Under the DSR operation conditions, R is limited in the range from 4 to 31. This phenomenon could be explained as follows: when the ratio R is less than 4, the nonlinear birefringence resulted from an asymmetric peak power distribution between the two principal axes is negligible relative to the linear birefringence. The walk-off effect induced by the intrinsic linear birefringence thereby results in the separation of the two polarization components and no stable DSR pulse can be formed in the cavity. On the other hand, when the ratio R is greater than 31, the peak power of the fast-axis component is much more intense than that of the slow-axis one. The pulse is approximately served as a linearly polarized light propagating along the fiber. In this case, the NPR effect is disabled and mode-locked pulses could not be formed. Furthermore, Fig. 9 shows that R is almost independent of the orientation angle φ and varies with θ. It should be noted that the lower and upper limits of the ratio R could be changed by adjusting the cavity length and dispersion of our proposed laser.

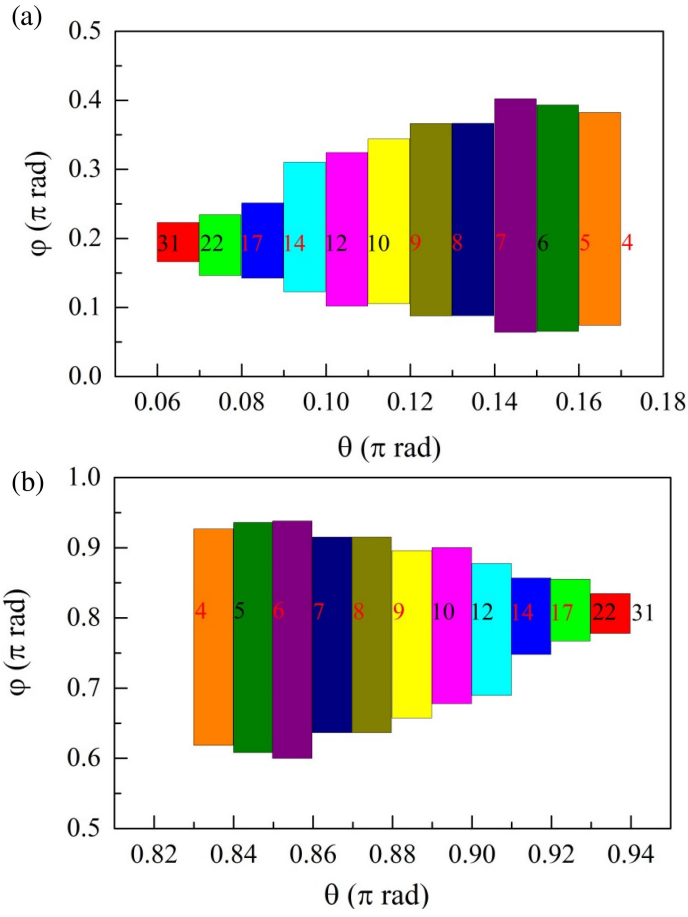

Fig. 9. The peak power ratio of the two components in the DSR pulse as a function of orientation angles θ and φ. (a) Zoomed in view of the red region in Fig. 8. (b) Zoomed in view of the blue region in Fig. 8. The contour lines with numbers in panels (a) and (b) denote the peak power ratio of the two components.

4. Conclusion

A numerical investigation on the vector nature of DSR pulses in an ANDi Yb-doped fiber laser mode-locked by the NPR technique has been performed. Through calculating the polarization ellipses of the DSR pulse inside the laser cavity, it has been shown that the polarization state changes, as both the orientation angle and ellipticity of the polarization ellipse vary during the propagation. The features of pulse polarization have also been displayed on the Poincaré sphere. The impact of nonlinear birefringence on the polarization evolution has been analyzed. The DSR pulse exhibits a unique internal polarization behavior. Its flat-top part acquires a nearly fixed polarization state, whereas the edges feature polarization states that vary with time. We have also found that the peak power ratio of the two polarization modes in the pulse is limited in the range from 4 to 31. Our simulation results give an insight into the polarization properties of DSR pulses in mode-locked fiber lasers involving polarization-dependent devices.

References

[1] U. Keller, "Recent developments in compact ultrafast lasers," *Nature*, vol. 424, no. 6950, pp. 831–838, Aug. 2003.
[2] L. F. Mollenauer, R. H. Stolen, and J. P. Gordon, "Experimental observation of picosecond pulse narrowing and solitons in optical fibers," *Phys. Rev. Lett.*, vol. 45, no. 13, pp. 1095–1098, Sep. 1980.

[3] L. E. Nelson, D. J. Jones, K. Tamura, H. A. Haus, and E. P. Ippen, "Ultrashort-pulse fiber ring lasers, " *Appl. Phys. B*, vol. 65, no. 2, pp. 277–294, Apr. 1997.
[4] K. Tamura, E. P. Ippen, H. A. Haus, and L. E. Nelson, "77-fs pulse generation from a stretched-pulse mode-locked all-fiber ring laser," *Opt. Lett.*, vol. 18, no. 13, pp. 1080–1082, Jul. 1993.
[5] W. H. Renninger, A. Chong, and F. W. Wise, "Dissipative solitons in normal-dispersion fiber lasers," *Phys. Rev. A*, vol. 77, no. 2, Feb. 2008, Art. no. 023814.
[6] W. Chang, A. Ankiewicz, J. M. Soto-Crespo, and N. Akhmediev, "Dissipative soliton resonances," *Phys. Rev. A*, vol. 78, no. 2, Aug. 2008, Art. no. 023830.
[7] W. Chang, A. Ankiewicz, J. M. Soto-Crespo, and N. Akhmediev, "Dissipative soliton resonances in laser models with parameter management," *J. Opt. Soc. Amer. B*, vol. 25, no. 12, pp. 1972–1977, Nov. 2008.
[8] R. W. Chang, J. M. Soto-Crespo, A. Ankiewicz, and N. Akhmediev, "Dissipative soliton resonances in the anomalous dispersion regime," *Phys. Rev. A*, vol. 79, no. 3, Mar. 2009, Art. no. 033840.
[9] A. E. Ding, P. Grelu, and J. N. Kutz, "Dissipative soliton resonance in a passively mode-locked fiber laser," *Opt. Lett.*, vol. 36, no. 7, pp. 1146–1148, Apr. 2011.
[10] V. A. Komarov, F. Amrani, A. Dmitriev, K. Komarov, and F. Sanche, "Competition and coexistence of ultrashort pulses in passive mode-locked lasers under dissipative-soliton-resonance conditions," *Phys. Rev. A*, vol. 87, no. 2, Feb. 2013, Art. no. 023838.
[11] W. Du, H. Li, J. Li, P. Wang, S. Zhang, and Y. Liu, "Mechanism of dissipative-soliton-resonance generation in fiber laser mode-locked by real saturable absorber," *Opt. Exp.*, vol. 26, no. 16, pp. 21314–21323, Aug. 2018.
[12] Z. Cheng, H. Li, and P. Wang, "Simulation of generation of dissipative soliton, dissipative soliton resonance and noise-like pulse in Yb-doped mode-locked fiber lasers," *Opt. Exp.*, vol. 23, no. 5, pp. 5972–5981, Feb. 2015.
[13] D. Li, D. Tang, L. Zhao, and D. Shen, "Mechanism of dissipative-soliton-resonance generation in passively mode-locked all-normal-dispersion fiber lasers," *J. Lightw. Technol.*, vol. 33, no. 18, pp. 3781–3787, Sep. 2015.
[14] X. Wu, D. Y. Tang, H. Zhang, and L. M. Zhao, "Dissipative soliton resonance in an all-normal-dispersion erbium-doped fiber laser," *Opt. Exp.*, vol. 17, no. 7, pp. 5580–5584, Mar. 2009.
[15] L. Duan, X. Liu, D. Mao, L. Wang, and G. Wang, "Experimental observation of dissipative soliton resonance in an anomalous-dispersion fiber laser," *Opt. Exp.*, vol. 20, no. 1, pp. 265–270, Jan. 2012.
[16] J. Zhao *et al.*, "100 W dissipative soliton resonances from a thulium-doped double-clad all-fiber-format MOPA system," *Opt. Exp.*, vol. 24, no. 11, pp. 12072–12081, May 2016.
[17] K. Krzempek and K. Abramski, "6.5 μJ pulses from a compact dissipative soliton resonance mode-locked erbium-ytterbium double clad laser," *Laser Phys. Lett.*, vol. 14, no. 1, Nov. 2017, Art. no. 015101.
[18] N. Zhao *et al.*, "Dual-wavelength rectangular pulse Yb-doped fiber laser using a microfiber-based graphene saturable absorber," *Opt. Exp.*, vol. 22, no. 9, pp. 10906–10913, May 2014.
[19] Z. Cheng, H. Li, H. Shi, J. Ren, Q. H. Yang, and P. Wang, "Dissipative soliton resonance and reverse saturable absorption in graphene oxide mode-locked all-normal-dispersion Yb-doped fiber laser," *Opt. Exp.*, vol. 23, no. 6, pp. 7000–7006, Mar. 2015.
[20] H. Yang and X. Liu, "WS_2-clad microfiber saturable absorber for high-energy rectangular pulse fiber laser," *IEEE J. Sel. Top. Quantum*, vol. 24, no. 3, Jun. 2018, Art. no. 0900807.
[21] L. M. Zhao, D. Y. Tang, H. Zhang, X. Wu, and N. Xiang, "Soliton trapping in fiber lasers," *Opt. Exp.*, vol. 16, no. 13, pp. 9528–9533, Jun. 2008.
[22] L. M. Zhao, D. Y. Tang, X. Wu, and H. Zhang, "Dissipative soliton trapping in normal dispersion-fiber lasers," *Opt. Lett.*, vol. 35, no. 11, pp. 1902–1904, Jun. 2010.
[23] L. M. Zhao, D. Y. Tang, H. Zhang, and X. Wu, "Polarization rotation locking of vector solitons in a fiber ring laser," *Opt. Exp.*, vol. 16, no. 14, pp. 10053–10058, Jul. 2008.
[24] M. Liu, A. P. Luo, Z. C. Luo, and W. C. Xu, "Dynamic trapping of a polarization rotation vector soliton in a fiber laser," *Opt. Lett.*, vol. 42, no. 2, pp. 330–333, Jan. 2017.
[25] D. Y. Tang, H. Zhang, L. M. Zhao, and X. Wu, "Observation of high-order polarization-locked vector solitons in a fiber laser," *Phys. Rev. Lett.*, vol. 101, no. 15, Oct. 2008, Art. no. 153904.
[26] L. M. Zhao, D. Y. Tang, X. Wu, H. Zhang, and H. Y. Tam, "Coexistence of polarization-locked and polarization-rotating vector solitons in a fiber laser with SESAM," *Opt. Lett.*, vol. 34, no. 20, pp. 3059–3061, Oct. 2009.
[27] Z. C Luo *et al.*, "Vector dissipative soliton resonance in a fiber laser," *Opt. Exp.*, vol. 21, no. 8, pp. 10199–10204, Apr. 2013.
[28] D. Li, D. Shen, L. Li, D. Tang, L. Su, and L. Zhao, "Internal polarization dynamics of vector dissipative-soliton-resonance pulses in normal dispersion fiber lasers," *Opt. Lett.*, vol. 43, no. 6, pp. 1222–1225, Mar. 2018.
[29] D. Y. Tang, L. M. Zhao, B. Zhao, and A. Q. Liu, "Mechanism of multisoliton formation and soliton energy quantization in passively mode-locked fiber lasers," *Phys. Rev. A*, vol. 72, no. 4, Oct. 2005, Art. no. 043816.
[30] J. Wu, D. Y. Tang, L. M. Zhao, and C. C. Chan, "Soliton polarization dynamics in fiber lasers passively mode-locked by the nonlinear polarization rotation technique," *Phys. Rev. E*, vol. 74, no. 4, Oct. 2006, Art. no. 046605.
[31] X. Liu, "Pulse evolution without wave breaking in a strongly dissipative-dispersive laser system," *Phys. Rev. A.*, vol. 81, no. 5, May 2010, Art. no. 053819.